Arch. Metall. Mater. **68** (2023), 3, 1165-1170

DOI: https://doi.org/10.24425/amm.2023.145489

W. MAZIARZ[1*], A. KOLANO-BURIAN[2], M. KOWALCZYK[3], P. BŁYSKUN[3], R. CHULIST[1], P. CZAJA[1], M. SZLEZYNGER[1], A. WÓJCIK[1]

TEM, HREM, L-TEM STUDIES OF Fe-BASED SOFT MAGNETIC MELT-SPUN RIBBONS SUBJECTED TO ULTRA-RAPID ANNEALING PROCESS

In the present work, we performed the ultra-rapid annealing (URA) process for amorphous $Fe_{78}Ni_8B_{14}$ melt-spun ribbons in order to obtain fine excellent microstructure assuring the best soft magnetic properties. Several microscopic methods mainly based on transmission electron microscopy (TEM) and Lorentz TEM (L-TEM) were applied for detailed studies of the microstructure and magnetic domains structure. The investigation revealed that the optimized parameters of the URA process (500°C/0.5-5 s) lead to outstanding soft magnetic properties. A mixture containing close to 50% amorphous phase and 50% α-Fe nanocrystals of size up to 30 nm has been already obtained after annealing for 3 s. These annealing conditions appear to be the most suitable in terms of microstructure providing the best magnetic properties.

Keywords: Soft magnetic materials; ultra-rapid annealing; microstructure; magnetic domain structure; TEM; L-TEM

1. Introduction

Nowadays, due to the prevention of global warming and resource saving, intensified electricity saving is required. One of the examples is a reduction of losses in transformers by using soft magnetic materials. Especially, amorphous and nanocrystalline alloys in form of melt-spun ribbons have lower hysteresis loss than conventional alloys such as silicon steel sheets, due to their microstructure, in which the magnetization is more easily rotated using applied magnetic fields. They are also known to have low eddy current losses, due to high electric resistance and formability to a thickness of approximately 25 μm. Thus, many efforts have been made to improve the magnetic properties of different groups of soft magnetic materials like Fe-Si-B-Nb-Cu (FINEMET) [1], Fe-M-B (NANOPERM) [2-6], Fe-Co-M-B (HITPERM; M = Nb, Zr, Hf) [7], Fe-Co-Nb-B-P (PYROPERM) [8] and FeNi-based [9-12]. Soft magnetic nanocrystalline alloys are often obtained by thermal annealing of amorphous alloys, however, their magnetic properties are sensitive to chemical composition as well as microstructure. Nanocomposites consisting of α-Fe crystallites with sizes smaller than 35 nm, surrounded by an amorphous matrix showed low coercivity and high permeability [13]. This behaviour is based on a random anisotropy model in which the averaging of magnetocrystalline anisotropy plays a key role. Thus, for this reason, α-Fe crystallites have to be smaller than the natural exchange length, which equals 35 nm for Fe [13]. A high nucleation density is necessary for achieving a uniform and dense nanocrystalline structure. Sharma et al. [14] found that the grain size during crystallization can be controlled not by the diffusion rate, but by the growth harmony between the pre-existing and newly formed nuclei if sufficiently high heating rates are ensured. There is so-called critical temperature above which a larger number of nuclei exists. It was found that the best nanocrystalline structure ensuring good soft magnetic properties can be obtained when both the pre-existing nuclei/Fe-rich places and newly formed nuclei grow together. However, it happens only when high heating rates during annealing are used. A large number of nuclei together with lack of diffusion barrier for Fe lead to uniform crystallization of α-Fe crystals. Moreover, the high density of α-Fe nuclei conduces to competition for growth and consequently provides the reduction of crystallites size even down to 20 nm. Additionally, magnetic domain shape and size as well as the movement of magnetic domain walls and their width have an influence on magnetic anisotropy [15,16]. Their

[1] INSTITUTE OF METALLURGY AND MATERIALS SCIENCE, POLISH ACADEMY OF SCIENCES, 25 REYMONTA STR., 30-059 KRAKOW, POLAND
[2] LUKASIEWICZ RESEARCH NETWORK – INSTITUTE OF NON-FERROUS METALS, 5 GENERAŁA JÓZEFA SOWIŃSKIEGO STR., 44-121 GLIWICE, POLAND
[3] WARSAW UNIVERSITY OF TECHNOLOGY, THE FACULTY OF MATERIALS SCIENCE AND ENGINEERING, 141 WOŁOSKA STR., 02-507 WARSZAWA, POLAND

* Corresponding author: w.maziarz@imim.pl

© 2023. The Author(s). This is an open-access article distributed under the terms of the Creative Commons Attribution-NonCommercial License (CC BY-NC 4.0, https://creativecommons.org/licenses/by-nc/4.0/deed.en which permits the use, redistribution of the material in any medium or format, transforming and building upon the material, provided that the article is properly cited, the use is noncommercial, and no modifications or adaptations are made.

characterisation can be successfully performed with the use of TEM Lorentz microscopy in the Fresnel mode. Therefore, in this work, an attempt is made to study the relationship between microstructure, magnetic domains structure and soft magnetic properties in Fe-Ni-B melt-spun ribbons subjected to ultra-rapid annealing (URA) process.

2. Experimental procedure

Alloy with the nominal composition $Fe_{78}Ni_8B_{14}$ (at. %) was prepared by induction cast in quantity of about 2 kg from pure (3N) Fe, Ni elements and master FeB_{18} alloy. Then, the ingot was melted by induction at 1250°C in quartz tubes and ejected with 26-28 kPa overpressure from the quartz tube to a copper wheel rotating with 1260 rpm in order to produce the melt-spun ribbons. The ribbons were ultra-rapidly annealed at 773 K for 0.5÷14 s with a heating rate of ~100 K/s. The URA process was performed in a specially designed and constructed apparatus, more details about this device can be found elsewhere [17]. The microstructure of ribbons was examined using a Tecnai G2 Transmission Electron Microscope (TEM) and magnetic domain structure was analysed by Lorentz TEM (L-TEM) with use of Thermo-Scientific Titan Themis x-FEGThemis Cs corrected TEM microscope. Thin lamella for TEM was prepared by focused ion beam (FIB) technique using Thermo-Scientific SCIOS 2 DualBeam. Magnetic measurements were performed in a hysteresis loop tracer, specially designed for soft magnetic materials in the ribbon shape attachment. Properties of extremely soft magnetic materials were measured with high sensitivity in the magnetic field with a range of ±660 A/m. The measuring unit was based on the idea described by Kulik et al. [18]. The crystal structure of the ribbons after URA process were analysed by the X-ray diffraction using $Cu_{K\alpha}$ radiation and the Rietveld refinement was applied for the volume fraction of amorphous and nanocrystalline phases calculation.

3. Results and discussion

The investigation began with an analysis of the microstructure of as spun $Fe_{78}Ni_8B_{14}$ ribbons. Fig. 1 presents a set of TEM bright field (BF), dark field (DF) images and corresponding selected area electron diffraction (SAED) pattern. One can see a fully amorphous structure manifested by the two diffused rings in the SAED pattern. DF microstructure performed from part of first diffused ring (indicated by the circle) is also fully amorphous however, some individual bright spots can be recognized.

The observations with the use of high resolution electron microscopy (HREM) presented in Fig. 2 allowed to identify an additional microstructural phenomenon. The Inverse Fast Fourier transform (IFFT) image shows that besides the typical amorphous microstructure, several areas with an ordered configuration of atom columns usually considered in literature as short-range ordering (SRO) can be observed. In the magnified insert of IFFT

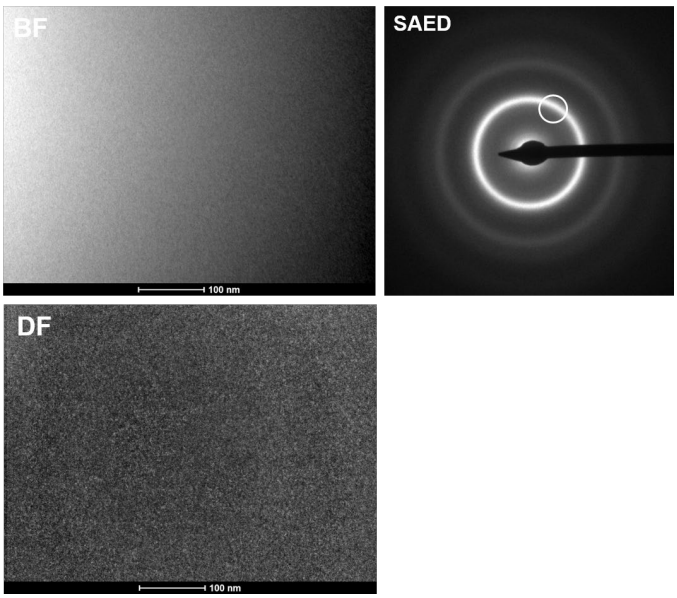

Fig. 1. Set of BF, DF microstructures and corresponding SAED pattern of as spun ribbon

image one can see SRO with the typical eucentric onion-like contrast. According to Sato et al. [19] this type of SRO can be considered as [111]-oriented bcc-Fe-like clusters with a size of about 1 nm. The structural heterogeneity of the melt-spun $Fe_{85.2}Si_2B_8P_4Cu_{0.8}$ alloy by spherical aberration (Cs) corrected high resolution transmission electron microscopy and revealed a formation of a hetero-amorphous structure including high-density crystalline clusters with the high Fe content was studied. The size of the clusters is typically ~1 nm in diameter. A part of these clusters is bcc-Fe-like in respect of interplanar spacing and symmetry of nanobeam electron diffraction patterns as well as atomic image contrast. These clusters can be considered as "pre-existing" bcc-Fe clusters, which would play a key role in the formation process of high-density α-Fe nanocrystals with excellent soft magnetic properties during ultra-rapid annealing.

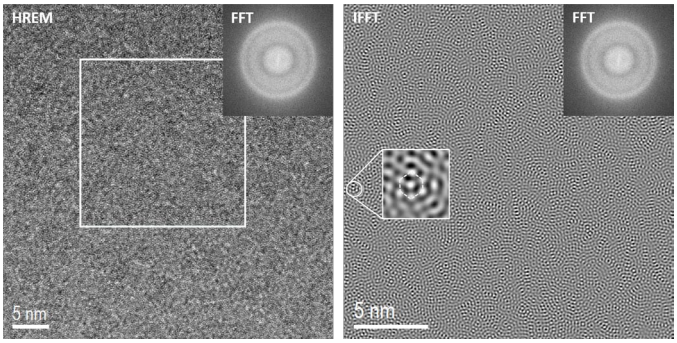

Fig. 2. HREM image and corresponding IFFT and FFT images of as spun ribbon

The crystallization process after different times of annealing was studied using X-ray diffraction. Fig. 3 presents a set of diffraction patterns recorded after different times of ultra-rapid annealing, whereas in TABLE 1 the volume fraction of crys-

talline phase formed after different time and calculated using Rietveld refinement can be observed. One can see the mixture of nanocrystalline bcc α-(Fe) and amorphous phases is formed already after 0.5 s of annealing with the volume fraction of the crystalline phase of about 40%. Increasing the annealing time up to 5 s causes the increase of volume fraction of the crystalline phase up to about 52%. Further elongation of annealing time causes crystallization of nonmagnetic Fe_2B phase visible after 8 s both in the X-ray diffraction patterns and crystalline phase content. One can see the additional peaks corresponding to the Fe_2B phase and a significant jump in the fraction of crystalline phase up to about 64%. After 14 s of annealing almost fully crystalline microstructure is formed.

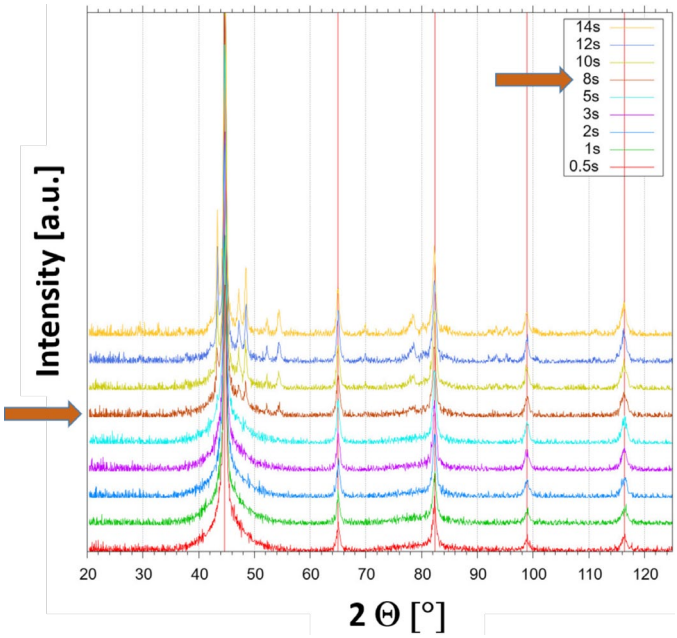

Fig. 3. Set of X-ray diffraction pattern recorded after different time of ultra-rapid annealing of $Fe_{78}Ni_8B_{14}$ amorphous ribbon

TABLE 1

Volume fraction of crystalline phase formed after different time calculated using Rietveld refinement

$t_{annealing}$ (s)	0.5	1	2	3	5	8	10	12	14
$V_{crystalline}$ (%)	40.2	41.5	50.6	52.6	52.1	64.2	74.5	85.0	91.5

The changes of crystal structure and volume fraction of nanocrystalline and amorphous phases have a strong influence on the soft magnetic properties of investigated ribbon. Fig. 4 presents hysteresis loops recorded for $Fe_{78}Ni_8B_{14}$ ribbon after different annealing times. Two ranges of annealing time strongly affect the soft magnetic properties can be distinguished. Between 0.5 and 5 s the magnetisation saturation up to 1.5 T is reached with a small coercivity, whereas in the range from 8 up to 14 s magnetisation saturation significantly drops down to about 1.3 T and not full magnetization saturation occurs even in the 5000 A/m magnetic field. Simultaneously, in this annealing time region coercivity increases up to about 500 A/m. These results, especially concerning the annealing time are in good agreement with the crystal structure investigations, but also the microstructure and magnetic domain structure have an impact on magnetocrystalline anisotropy and coercivity. For this reason, microstructure investigations were performed using a TEM conducting observation in different modes. As can be noticed the best soft magnetic properties (low coercivity, high magnetization saturation) have been obtained for ribbons showing 50 vol.% of α-Fe crystalline phase with the crystallites size of about 30 nm (see TEM results). Fig. 5 presents two examples of microstructures of ribbons annealed for 1 and 14 s. The homogenous nanocrystalline microstructure of bcc α-(Fe) solid solution confirmed by SAED can be observed in ribbon annealed for 1 s.

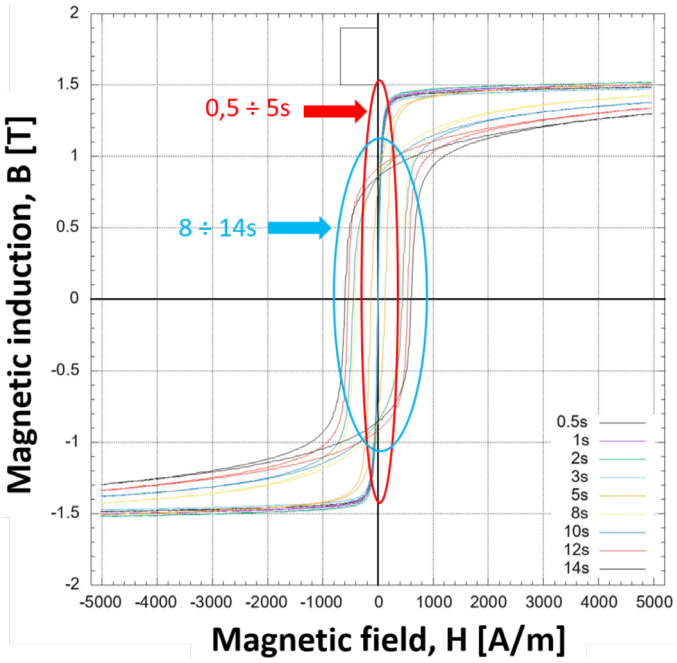

Fig. 4. Hysteresis loops of $Fe_{78}Ni_8B_{14}$ ribbons after different time holding during URA process

DF image taken from part of $(110)_{\alpha\text{-}Fe}$ ring shows crystallites of size of about 15 nm. In contrary, in the case of ribbon annealed for 14 s almost more than double increase of crystallites size of α-(Fe, Ni) solid solution up to about 36 nm can be observed as well as additional individual spots presented in the SEAD suggest the crystallization of boride Fe_2B. DF images recorded from the part of $(110)_{\alpha\text{-}Fe}$ ring and $(310)_{Fe2B}$ diffraction spot reveal significant differences in size and quantity of these individual crystallites. As was mentioned before, the URA process leads to the formation of a mixture of amorphous and nanocrystalline microstructure (TABLE 1). Due to the diffraction contrast in the BF images, it is difficult to recognise an amorphous part of microstructure and also places where borides are located. Therefore, additional microstructure observations in the high resolution mode were performed.

Fig. 6 and 7 present the results of HREM investigations for ribbons annealed for 1 and 14 s, respectively. In the case of ribbon annealed for 1 s, α-Fe particle of size of about 15 nm and

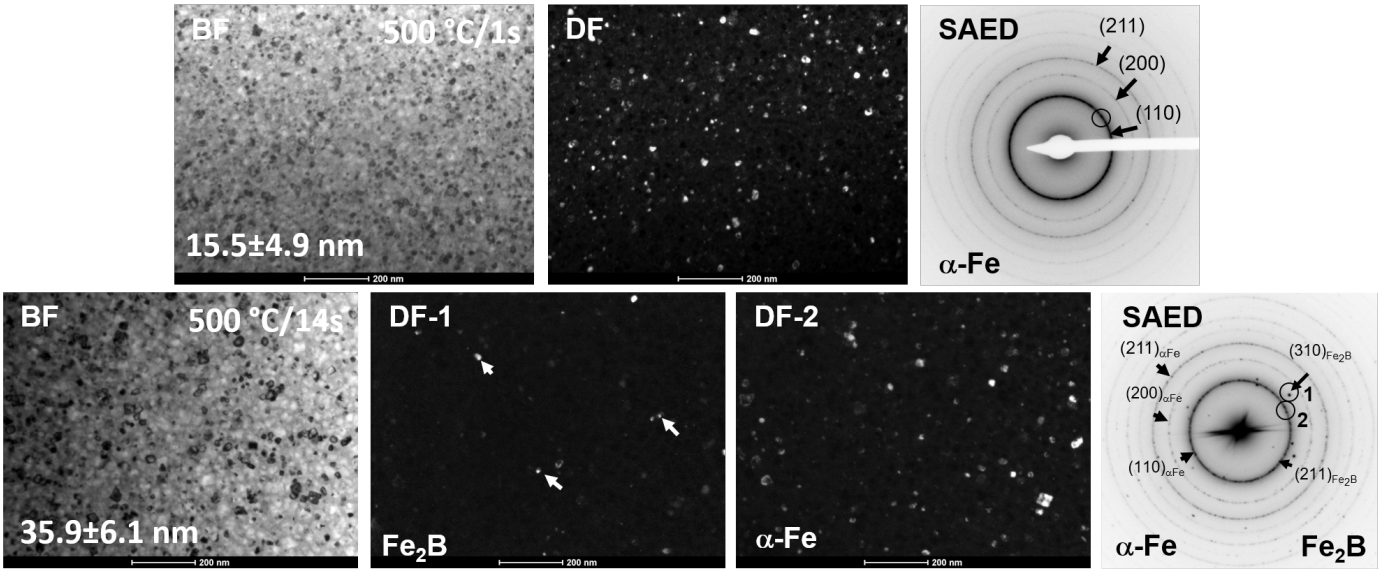

Fig. 5. BF, DF microstructures and corresponding SAED patterns of ribbons annealed for 1 (upper row) and 14 s (below row)

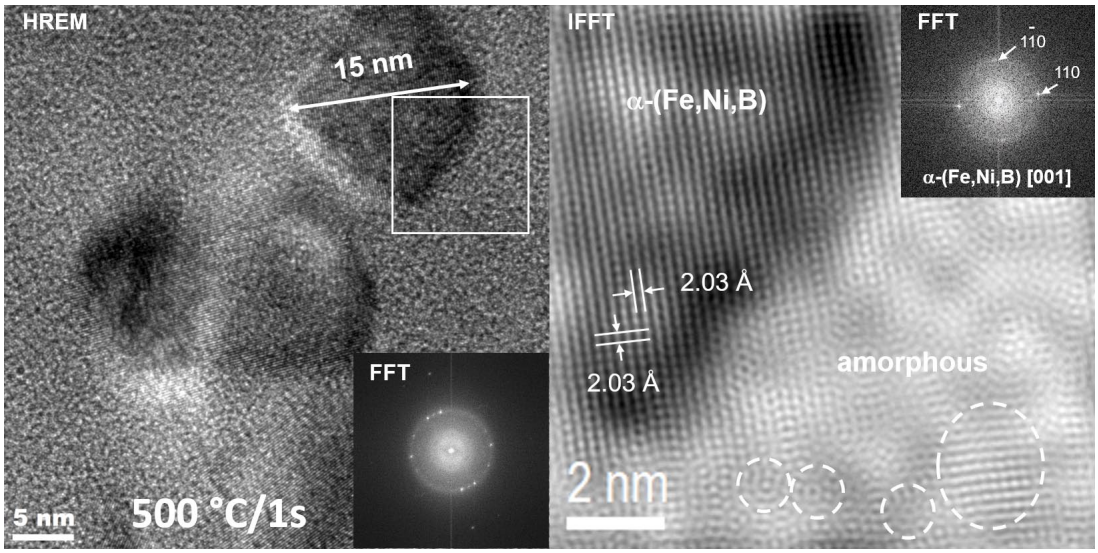

Fig. 6. HREM image and corresponding FFT and IFFT images for $Fe_{78}Ni_8B_{14}$ ribbon annealed for 1 s

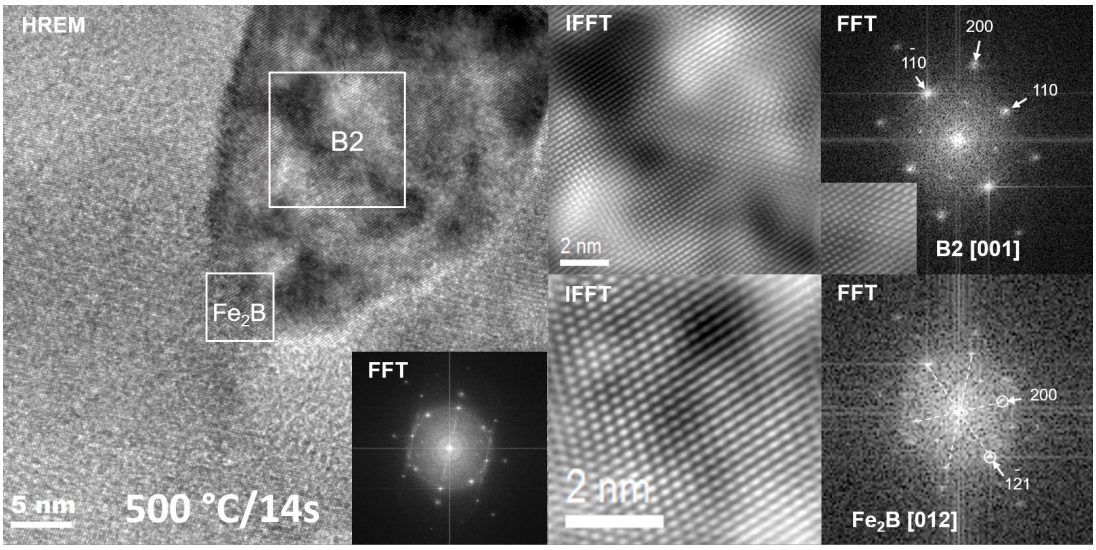

Fig. 7. HREM image and corresponding FFT and IFFT images for $Fe_{78}Ni_8B_{14}$ ribbon annealed for 14 s

cuboidal shape embedded in the amorphous matrix can be seen in HREM image. Fast Fourier Transform (FFT) image (in the coroner of HREM) performed from the whole area of HREM image reveals a single diffused ring with several individual spots corresponding to the amorphous and nanocrystalline phases, respectively. Detailed analysis taken from the interface between amorphous and nanocrystalline (indicated by the withe square) phases can be seen in IFFT image obtained after masking and filtering procedure. The nanocrystalline α-(Fe,Ni) particle with the [001] zone axis orientation is neighbouring with the amorphous matrix in which a high density of [111] and [001] oriented bcc-Fe-like clusters with a size of about 1 and 2 nm, respectively, was noticed.

This can suggest that during annealing for 1s at 500°C after rapid heating (100 K/s) both crystallization of α-Fe nanocrystalline phase and formation of oriented bcc-Fe-like clusters occurs. A distinctly different microstructure occurs in the ribbon annealed for 14 s. HREM image, Fig. 7, shows that part of ordered B2 type particle with [001] zone axis manifested by the additional spots in ½ distance of (200) planes, neighbouring with the amorphous matrix. In the FFT image (in the corner of HREM) performed from the whole area of HREM, a weak diffused ring corresponding to amorphous phase and several individual spots can be distinguish. Detailed analysis carried out in the different areas by using ROI (Range Of Interest) tools allowed to determine small particles of a size of about 5 nm, which can be considered as Fe_2B phase located on the edge of B2 particle. This can suggest that nucleation of Fe_2B particles occurs in energetically privileged interfaces between α-Fe solid solution and amorphous phase. Simultaneously, a part of the area where α-Fe solid solution particles neighbouring with the newly forming Fe_2B particle have tendency to ordering B2 type due to depletion in B and Fe.

Magnetic domains microstructure have been examined by the TEM Lorentz microscopy with the use of Fresnel mode. Fig. 8 shows Lorentz microscope images and reconstruction of magnetic domains in the amorphous as cast ribbon (upper row) and (bottom row) annealed at 500°C/1 s. Images observed in Fresnel mode show magnetic domain boundaries as white and black bands like those indicated by W1 and W2. One can see that magnetic domains of amorphous ribbons display a rather complicated domain wall distribution, resulting in the heterogeneous size and shape of domains. On the other hand, the ribbon after URA process performed for 1 s has a rather simple domain wall distribution. This causes especially existence of smaller amounts of pinning places of domain walls during their movement and finally reduces coercivity. Almost the same domain wall distribution was presented by Hiraoka et al. [16] in case of $Fe_{81}B_{15}Si_4$ amorphous specimen subjected to heat treatment with and without magnetic field. They found that heat-treatment with an external magnetic field increases the magnetic anisotropy, whereas heat treatments without magnetic field reduce the magnetic anisotropy. It is considered that the difference results from the alleviation of the strain field by heat treatment and the induced magnetic anisotropy caused by heat treatment with a magnetic field. Moreover, the initial observations of magnetic domain walls motion has been also performed by TEM showing that movement seems to be smoother, without pinning for ribbon partially crystallized comparing with the amorphous ones.

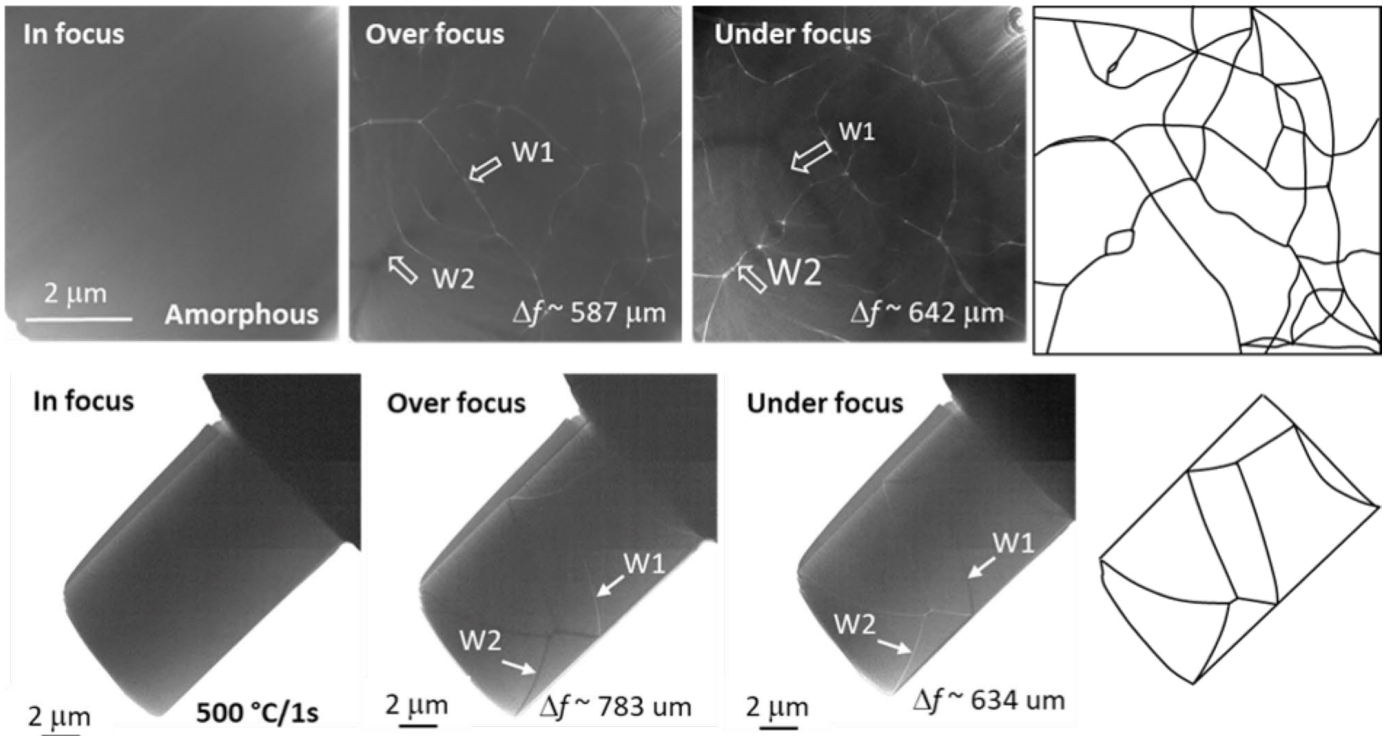

Fig. 8. TEM Lorentz microscope images and reconstructed images of magnetic domains of the amorphous as cast ribbon (upper row) and (bottom row) annealing at 500°C/1 s

4. Conclusions

The microstructure, magnetic properties and magnetic domain structure in $Fe_{78}Ni_8B_{14}$ specimen in the as-cast state and after URA were investigated by TEM, HREM and Lorentz microscopy. The results are summarized as follows:

1. Optimized parameters of the URA process of amorphous $Fe_{78}Ni_8B_{14}$ melt-spun ribbons lead to outstanding soft magnetic properties.
2. The mixture of close to 50:50 volume fraction of amorphous phase and α-Fe nanocrystals of size up to 30 nm, obtained after URA seems to be the most suitable microstructure providing the best magnetic properties.
3. The precipitation of Fe_2B phase after 8 s of URA process is the main cause of the deterioration of the soft magnetic properties.
4. The magnetic domain structure of ribbons after URA process was more straight comparing to the as spun ribbons. The magnetic domain walls motion in the specimens after URA seems to be smoother than in as spun due to the smaller amount of pinning places of domain walls. Moreover, URA process performed at 500°C/0.5-5 s allow to obtain homogenous, dense nanorystalline microstructure and consequently decreases the strain or stress fields in the as spun ribbons, resulting in narrow coercivity.

Acknowledgment

This research was founded by National Centre for Research and Development (POLAND) within the frame of project no TECHMATSTRATEG 2/410941/4/NCBR/2019

REFERENCES

[1] Y. Yoshizawa, S. Oguma, K. Yamauchi, J. Appl. Phys. **64**, 6044 (1988).

[2] A. Makino, T. Hatanai, A. Inoue, T. Masumoto, Mater. Sci. Eng. **A 226-228**, 594 (1997).

[3] K. Suzuki, A. Makino, A. Inoue, T. Masumoto, J. Appl. Phys. **74**, 3316 (1993).

[4] A. Hsiao, M.E. McHenry, D.E. Laughlin, M.J. Kramer, C. Ashe, T. Ohkubo, IEEE Trans. Magn. **38**, 3039 (2002).

[5] L. Hawelek, T. Warski, A. Radon, A. Pilsniak, W. Maziarz, M. Szlezynger, M. Kadziolka-Gawel, A. Kolano-Burian, Materials **14**, 7807 (2021).

[6] A. Wojcik, W. Maziarz, M. Kowalczyk, R. Chulist, M. Szlezynger, P. Czaja, L. Hawelek, P. Zackiewicz, P. Wlodarczyk, A. Kolano-Burian, Materials **13**, 1639 (2020).

[7] M.A. Willard, M.-Q. Haung, D.E. Laughlin, M.E. McHenry, J.O. Cross, V.G. Harris, C. Franchetti, J. Appl. Phys. **85**, 4421 (1999).

[8] A. Kolano-Burian, P. Zackiewicz, A. Grabias, A. Wojcik, W. Maziarz, M. Szlezynger, P. Wlodarczyk, M. Kowalczyk, L. Hawelek, Materials **14**, 3433 (2021).

[9] L. Hawelek, T. Warski, P. Wlodarczyk, M. Polak, P. Zackiewicz, W. Maziarz, A. Wojcik, M. Steczkowska-Kempka, A. Kolano-Burian, Materials **14**, (2021).

[10] N. Aronhime, E. Zoghlin, V. Keylin, X. Jin, P. Ohodnicki, M.E. McHenry, Scr. Mater. **142**, 133-137 (2018).

[11] N. Aronhime, V. DeGeorge, V. Keylin, P. Ohodnicki, M.E. McHenry, JOM **69**, 2164-2170 (2017).

[12] T. Warski, A. Radon, P. Zackiewicz, P. Wlodarczyk, M. Polak, A. Wojcik, W. Maziarz, A. Kolano-Burian, L. Hawelek, Materials **14**, 726 (2021).

[13] G. Herzer, Modern soft magnets: Amorphous and nanocrystalline materials, Acta Materialia **61**, 718-734 (2013).

[14] P. Sharma, X. Zhang, Y. Zhang, A. Makino, Scr. Mater. **95**, 3-6 (2015).

[15] K. Saito, H.S. Park, D. Shindo, Y. Yoshizawa, Journal of Magnetism and Magnetic Materials **305**, 304-309 (2006).

[16] M. Hiraoka, Z. Akase, D. Shindo, Y. Ogawa, Y. Yoshizawa, Materials Transactions **50**, 12, 2839-2843 (2009).

[17] A. Kolano-Burian, M. Kowalczyk, A. Grabias, A. Radoń, P. Błyskun, T. Warski, M. Karpiński, L. Hawelek, T. Kulik, Journal of Alloys and Compounds **921**, 165943 (2022).

[18] T. Kulik, H.T. Sevage, A.J. Hernando, Appl. Phys. **73**, 6855-6857 (1993).

[19] K. Sato, K. Takenaka, A. Makino, Y. Hirotsu, AIP Adv. **5**, 067166 (2015).